Visual Abstract

Degradation of the first frequency of an RC frame with damage levels

Quy Thue Nguyen
Faculty of Civil Engineering, Nguyen Tat Thanh University, Ho Chi Minh City, Vietnam
ntquy@ntt.edu.vn, nguyenthuequy@gmail.com, https://orcid.org/0000-0003-3436-8551

Ramazan Livaoğlu
Department of Civil Engineering, Bursa Uludağ University, Bursa City, Türkiye
rliva@uludag.edu.tr, http://orcid.org/0000-0001-8484-6027

ABSTRACT. Damage in RC structures causes the degradation of stiffness and frequency. In this study, the relationship between the two coefficients and damage severities is numerically investigated considering a three-dimensional (3D) RC frame in which the concrete damage plasticity model (CDPM) and the elastoplastic model are selected for concrete and reinforcements, respectively. Crack propagation is obtained utilizing a nonlinear static pushover analysis (NSPA). After pushing, according to the base shear force versus top displacement curve, the bending stiffness of the structure is determined rapidly based on the first derivative of the relationship. Thereafter, the degradation of the first frequency is obtained based on the derivative of the nonlinear curve of stiffness, the second derivative of the force-displacement curve viz. As a result, it is observed that the degradation of the first frequency of the RC frame is proportional to the severity of damage but not linearly. More significant damage, a more profound decrease in the frequency. Particularly, the frequency of the frame reduces gradually until the base shear force reaches 70% of the ultimate value at which the parameter is 60% of the healthy counterpart. After that, the reduction gets more significant when the bending capacity approaches the ultimate value.

KEYWORDS. Structural Integrity, Structural Health Monitoring, Natural Frequency, Concrete Damage Plasticity Model, Pushover Analysis.

OPEN ACCESS

Citation: Nguyen, Q. T., Livaoğlu, R., Degradation of the first frequency of an RC frame with damage levels, Frattura ed Integrità Strutturale, 64 (2023) 1-10.

Received: 02.11.2022
Accepted: 12.01.2023
Online first: 14.01.2023
Published: 01.04.2023

INTRODUCTION

Structural health monitoring (SHM) has been applied to control regularly the health of RC structures which have deteriorated having been subjected to a sudden loading (Khatir et al. [1]). Systems under service also undergo some faults as a consequence of environmental conditions or accidental events (Ho et al. [2]). It is vital for engineering

applications (Benaissa et al. [3]). Since maintenance and repair of existing structures are essentially required (Ho et al. [4]). Evaluating the vibrations of buildings possibly leads to an indication of the extent of faults that may transpire in the incoming earthquake events of as stated by Kristiawan et al. [5]. Khatir et al. [6] claimed that cracks are among the most commonly witnessed failure types in engineering structures and materials. Crack propagation plays a decisive role in the residual lifetime of any structure (Khatir and Wahab [7], Thobiani et al. [8]). After damage occurrence or crack presence, stiffness parameters of monitored structures reduce, leading to changes in terms of modal characteristics such as frequency and mode shape. Vibration-based damage detection methods have played an important role among current non-destructive evaluation testing techniques (Gillich et al. [9]). The modal information is targeted in various damage assessment methods (Gentile et al. [10], Tiachacht et al. [11], Saisi et al. [12], Iacovino et al. [13], Khatir et al. [14]). Compared to mode shape generations, frequency measurements are cheap, quickly conducted, and often reliable. Therefore, it has been focused on in literature. Non-destructive methods assessing the integrity of structures based on natural frequencies have been mentioned in many studies (Cerri and Vestroni [15], Yang and Wang [16]). Natural frequency is considered a diagnostic parameter in structural assessment procedures using vibration monitoring, particularly an analysis of periodical frequency in Salawu [17]. In general, natural frequency shifts are sensitive damage indicators of damage occurrence. Loss of the structural stiffness caused by the damage of materials directly leads to natural frequency degradation. It means the natural frequencies that are straightforwardly identified in practice contain information about the damage severities or declination of stiffness parameters of complicated structures like RC buildings. Hence, the relationship between the two parameters has also taken a lot of interest but not adequately. For instance, changes in resonant frequency with increasing loads of a simply supported RC beam with multiple cracks using different dynamic excitations for various damage levels were evaluated by Hamad et al. [18]. The author showed that at 30% of the ultimate load, the resonant frequency decreases an amount of 10% from the counterpart of the intact one and then gradually reduces. The amount of reduction is about 25% as the beam is loaded by 70% of the ultimate load. Targeting larger and more complicated structures than an RC beam, this current study is to investigate the fundamental frequency degradation due to damage severity of a 3D RC frame. More importantly, the proposed two-step derivative procedure allows us to figure out the full relationship between stiffness degradation and the fundamental frequency. From the authors' point of view, such a study has not been considered adequately. The suggested approach requires a full curvature of loading and top displacement but there are indeed some difficulties to set up an investigation on real specimens like RC frames. Hence, the investigation is conducted by simulating the RC frame whose materials have been validated in order to reach reliable results. Meanwhile, numerical investigations have taken interest from researchers such as Roumaissa et al. [19], Le Thanh et al. [20], Saadatmorad et al. [21], Shirazi et al. [22]. For more enormous and complex structures, the presented derivative procedure is promising for similar examinations on the frequency declination caused by damage, especially RC buildings regardless of numerical or experimental studies.

SIMPLE APPROACH TO INVESTIGATE FREQUENCY DEGRADATION

In SHM of RC buildings, structural damage causes degradation in terms of stiffness while the mass parameter keeps unchanged. Therefore, at each mode, the frequency degradation depends only on the stiffness parameter as seen in Eqn. 1, making it can be captured once the declination of stiffness is determined. Particularly, the natural frequency reduction is proportional to the square root of the stiffness coefficient degradation.

$$f = \frac{1}{2\pi}\sqrt{\frac{k}{m}} \tag{1}$$

Changes in terms of frequency caused by different damage severities on RC structures can be obtained completely considering its nonlinear behavior. The frequency degradation is then can be determined using the 2-step derivative as demonstrated in Fig. 1. Initially, a nonlinear static pushover analysis is implemented on monitored RC frames to capture the relationship between base-shear force versus top displacement. The relationship in a specific range is then formulated to build an original equation. Thereafter, the stiffness degradation according to damage levels is directly determined from the 1st derivative of the equation. The declination of the corresponding natural frequency is finally reached based on the 2nd derivative of the original formulation.

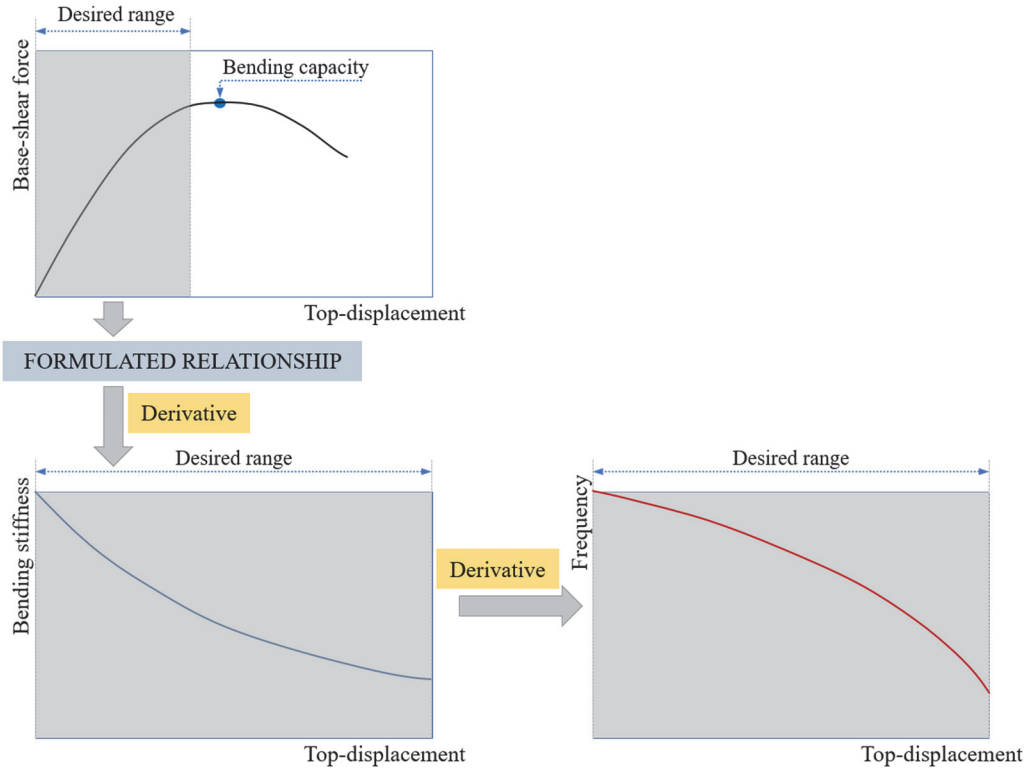

Figure 1: Flowchart of frequency degradation determination from NSPA.

MATERIAL SELECTION

Aiming at a realistic behavior of RC structures, especially at inelastic stages, the material models of concrete and reinforcement should be selected appropriately. In the commercial software, ABAQUS CAE®, the CDPM is conducted according to Kupfer et al. [23] and Lubliner et al. [24]. The software is capable of capturing the nonlinear behaviour of concrete due to a refined constitutive model of damage coupled with plasticity (see Batista da Costa et al. [25]). Nguyen and Livaoğlu [26] successfully validated the model using a four-point bending test on an RC beam conducted by Perera and Huerta [27]. Particularly, the required parameters utilized to define the CDPM (see Tab. 1) are built based on previous studies (Kupfer et al. [23], Ren et al. [28], and Najafgholipour et al. [29]). As demonstrated in Fig. 2, the uniaxial behavior in compression is exploited based on Hsu and Hsu [30] and Carreira [31] whereas the tensile regime is delineated following Aslani and Jowkarmeimandi [32]. In Fig. 2a, β is a parameter related to the shape of the compressive branch in the inelastic range, further information about this parameter can be followed in Carreira [31].

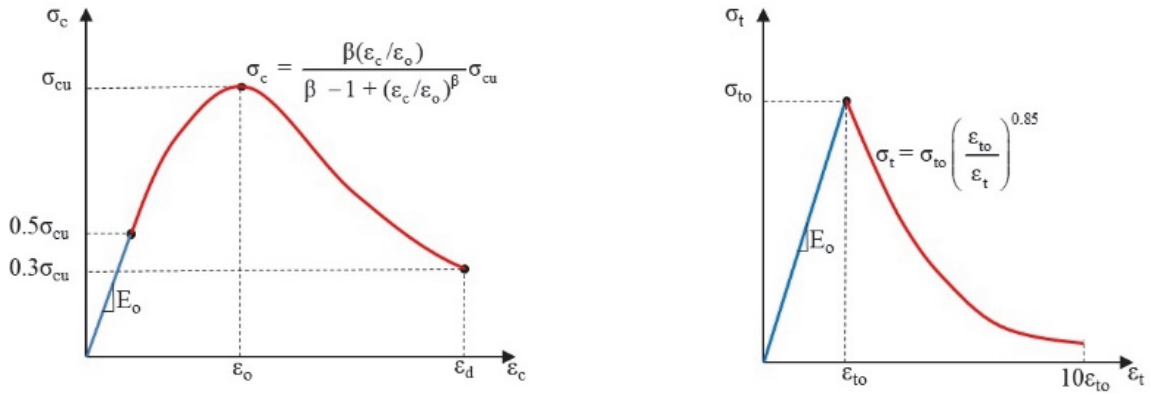

Figure 2: Uniaxial stress-strain curve of concrete (a) in compression and (b) in tension.

Parameter	Value
Dilation angle	35
Eccentricity	0.1
K	2/3
f_{b0}/f_{c0}	1.16
Viscosity parameter	0.007985

Table 1: Parameters of CDPM.

The mechanical properties of concrete whose compressive strength is 32 MPa are listed in Tab. 2. In particular, the Poisson's ratio is set as 0.18 according to Kupfer et al. [23] and Lee and Fenves [33]. The tensile capacity is indicated as 10% of the ultimate compressive strength according to Aslani and Jowkarmeimandi [32] but a percentage of 12 is selected since it leads to a good agreement with empirical data (see Nguyen and Livaoğlu [26]). On the other hand, the elastoplastic model is selected to define the reinforcements. The detailed mechanical characteristics of reinforcements are listed in Tab. 3.

Properties (cylindrical specimen at 28-day age)	C32
Ultimate compressive strength	32 MPa
Tensile capacity	3.84 MPa
Density	2.3 t/m^3
Elastic modulus	17953.3 MPa
Poisson's ratio	0.18

Table 2: Mechanical properties of concrete.

Properties	S510
Yielding strength	510 MPa
Density	7.85 t/m^3
Elastic modulus	210000 MPa
Poisson's ratio	0.3

Table 3: Mechanical properties of reinforcement.

Another verification of the material models is also conducted herein as another contribution of this study. Xiao [34] applied a concentrated load at the right center of a 1200-mm-square RC slab whose thickness is 150 mm as seen in Fig. 3a. The load-carrying capacity of the slab that depends on loading rates was examined. A detailed description of the experiment such as specimen properties, test setup and procedures, instrumentation, and can be followed in the original study. Some key information about the specimen is mentioned herein for a better understanding of the numerical model. The experiment is imitated in ABAQUS CAE® to verify the material models utilized in this current study based on the failure mechanism and the load carrying capacity of the slab under a monotonic pushing procedure. It should be noted that the aforementioned material models are also implemented to simulate the slab. The compressive strength of concrete is 42.9 MPa and the yield strength of reinforcing bars is 443 MPa. Although the classes of materials are different from those of the beam, they can be defined in the same manner as done for the beam.

In the experiment, the four sides of the slab were bolted to a supporting system using 24 high-tension bolts (6 ones for each side). Besides that, the supporting system is a 1200×1200 mm steel support composed of a series of H-shaped steel beams (Fig. 3b). The system was constrained to a strong floor with high-tension bolts to provide enough rigidity during testing. It is seen that bolting was chosen to constraint the supporting system to the floor below and the slab above it. It is assumed that a completely fixed boundary conditions of the slab may not be attained. Therefore, in the numerical model, two kinds of conditions were examined, simply supported and fully fixed. Similar to Nguyen and Livaoğlu [26], in the simulation, linear hexahedral elements of type C3D8R and linear line elements of type T3D2 were utilized to define concrete and reinforcements, respectively. The meshing size of 50 mm for both types of materials was defined. As a result, the numerical model of the slab is composed of 2628 elements and 3400 nodes. They are formed by 1728 C3D8R elements and 900 T3D2 elements.

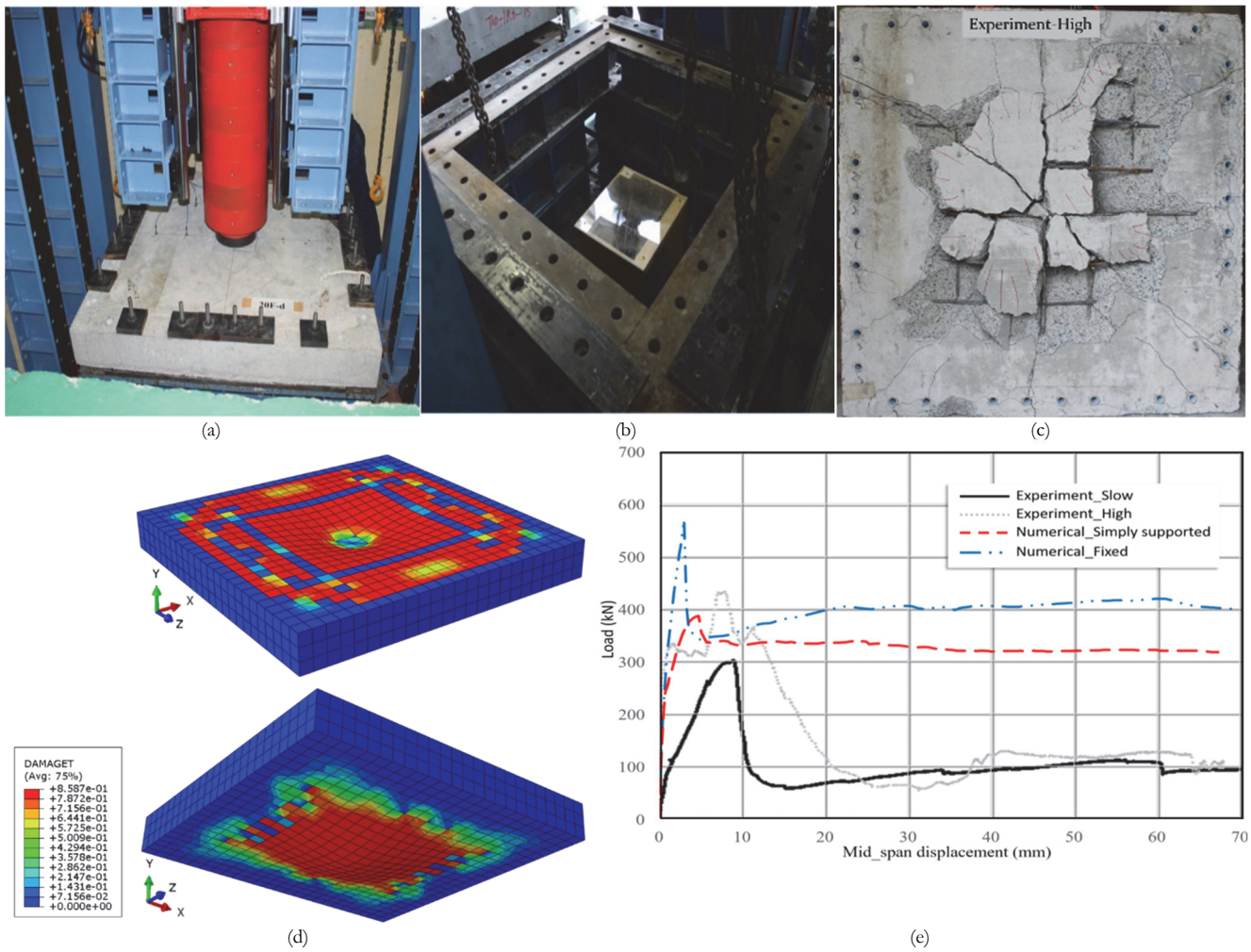

Figure 3: Verification of material models on a RC slab conducted by Xiao [34] (a) Test set up (b) Supporting system (c) Real damage mode (d) Numerical damage mode and (e) Comparison of load carrying capacity.

The bending capacity and damage mechanism are considered when comparing the experimental and numerical slabs. The real slab was pushed under different loading rates, a static loading rate of 0.0004 m/s (Experiment_Slow) and a high loading rate of 2 m/s (Experiment_High). Displacement sensors and load cells were arranged to collect the applied load and the movement of the mid-span of the slab during pushing. The damage mechanism captured at the low surface of the slab under Experiment_High is shown in Fig. 3c. On the other hand, damage is captured on the top and bottom of the numerical specimen in the case of fully fixed conditions as seen in Fig. 3d. It can be seen that damage mechanisms in the numerical and experimental specimens are in harmony with each other. Moreover, the nonlinear behavior of the two numerical cases is generally similar to that of Experiment_Slow as picturized in Fig. 3e. It initiates from a linear tendency and then gradually falls into a nonlinear range until reaching a peak followed by a significant downward trend. Subsequently, stagnation is witnessed. Meanwhile, dynamic effects were observed in the case of Experiment_High. The numerical result is in harmony with that of Experiment_Slow since the pushing procedure is defined in a Static Step. However, some disagreements are witnessed among them. The numerical specimens seem to be stiffer than the real one as seen in their linear range. Furthermore, the load-carrying capacity of the two numerical specimens is higher than that of Experiment_Slow, especially Numerical_Fixed. The issues may be attributed to many reasons. For example, the real boundary conditions in the real text may be different from the two cases defined in the simulation. Moreover, steel bolts arranged to restrict the real slab to the supporting system can be deformed during loading, especially under high levels, making the boundary condition of the real slab may change during testing. It is true that different boundary conditions possibly lead to significant deviation. Even with no change in the boundary conditions, the notably different behaviors of the two numerical models can be taken as an example. Although they perform approximately in the same tendency in the elastic stage, they start deviating when falling into the inelastic stage. The carrying capacity of Numerical_Simply supported is remarkably lower than that of Numerical_Fixed. More importantly, a perfect bond using “embedded constraint” is utilized to define the interaction

between concrete and reinforcements whereas reinforcing bars may delaminate from their surrounding concrete in practice, especially under high levels of loading. That directly lowers the carrying capacity of the actual slab compared to that of the numerical specimens. It can be concluded that although the result of the verification on the slab is not good as seen for that of the beam, it is not bad and does not contain any problematic issues. The above-mentioned deviation can be lessened considering the potential reasons but that is not the main target of this study. Hence, the selected material models are also acceptable for further investigation.

NUMERICAL SPECIMEN DESCRIPTION

A 3D RC frame is simulated in the commercial program as one solid body. The finished dimensions and cross-section of columns (300 mm x 300 mm) and beams (250 mm x 300 mm) are shown in Fig. 4. It is noted that in all cross-sections, there are 4 longitudinal reinforcing bars whose diameter is 14 mm. On the other hand, 8 mm is the diameter of stirrups that are placed with intervals of 150 mm for both columns and beams. The clear cover of the concrete is 26 mm. The bottom surfaces of the bases are completely fixed.

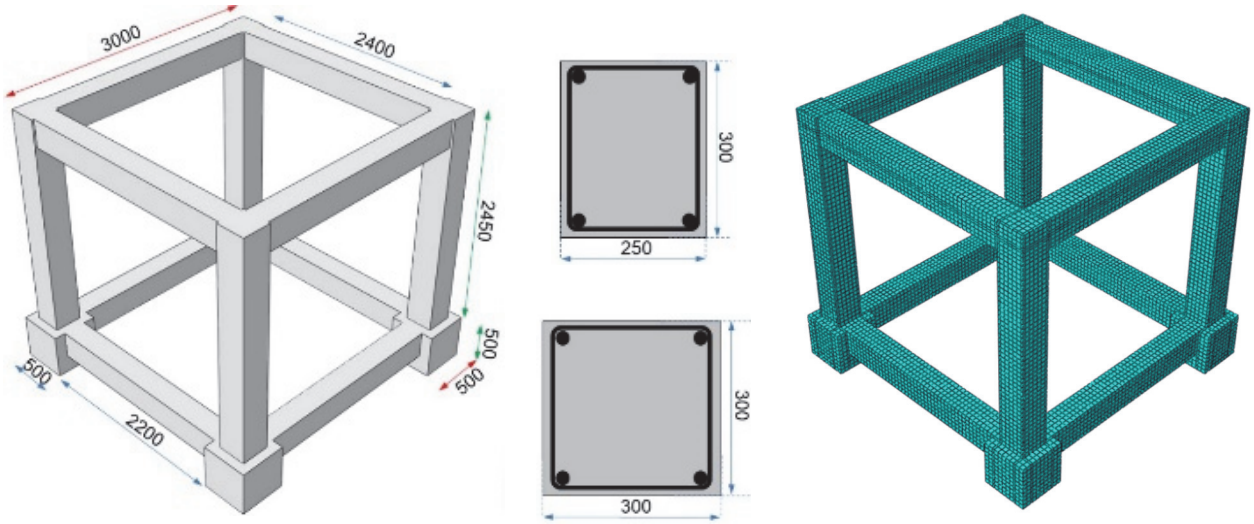

(a) (b) (c)

Figure 4: Numerical model (a) Finished dimensions, (b) beam and column sections, and (c) meshing.

NONLINEAR STATIC PUSHOVER ANALYSIS SET UP

The NSPA procedure as shown in Fig. 5a is defined in ABAQUS CAE® as a displacement-control procedure. It should be noted that the analysis consists of two main steps. Step 1 is used to account for the response against the constant normal loading as profoundly illustrated by the purple components. In particular, the value of the axial load of 5.97 N/mm² (equal to about 19% of the normal capacity of structural members) is imparted constantly in the Y-axis at the top of the four columns. The gravitational load is also considered in Y-axis in the same direction. It is noted that the effects of this loading are propagated into the next step. In Step 2, the structure is subjected to a monotonically pushing procedure, red components. In Fig. 5a, a monotonic lateral pushing procedure is applied on two columns with respect to the X-axis using a displacement control approach. the lateral displacement is applied incrementally until the drift ratio is equal to 3.5% as stipulated by ACI Committee 374.1 [35]. That makes the target of lateral displacement equal to 87.75mm. Step 1 works separately from Step 2 and then the results of the former step are propagated into the latter one. Moreover, during the both steps, the foot is restrained spatially by assigning the "fixed boundary condition" option to the surfaces at the bottom surfaces of the bases. In general, 50 mm x 50 mm x 50 mm size meshing is utilized to solid elements (see Fig. 4c) whereas the size of 50 mm is selected for truss elements. The numerical model is composed of 27796 linear hexahedral elements of type C3D8R for concrete and 7080 linear line elements of type T3D2 for reinforcements, producing 43896

nodes. After the determination of the base-shear force versus top lateral displacement, the displacement ductility factor of the RC frame can be determined in Fig. 5b according to Park [26].

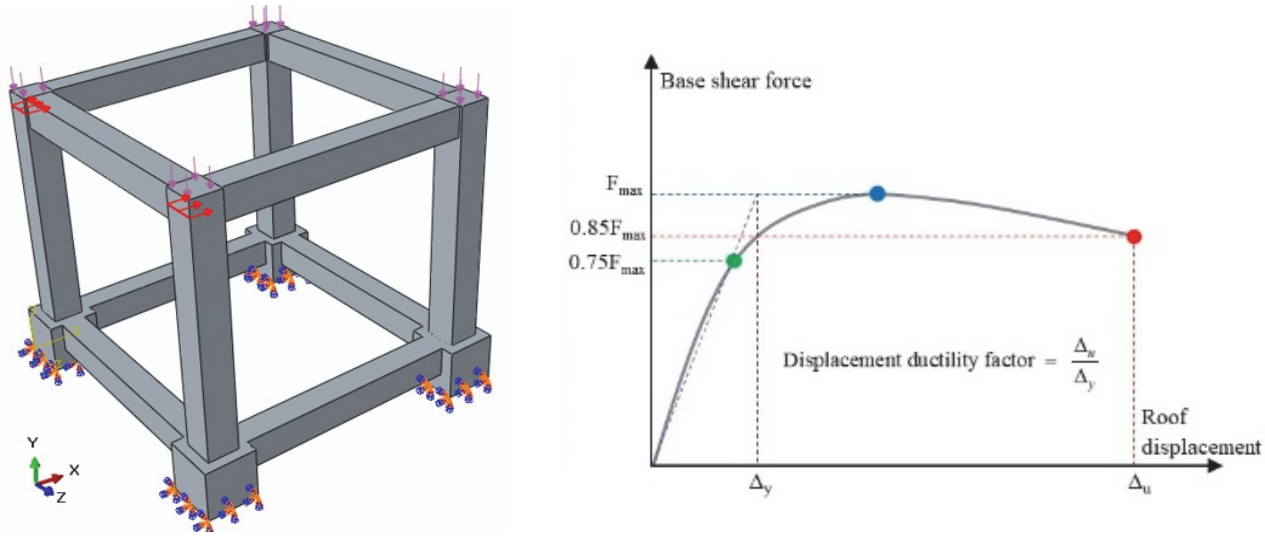

(a) (b)

Figure 5: Numerical NSPA (a) Test set up and (b) displacement ductility factor determination.

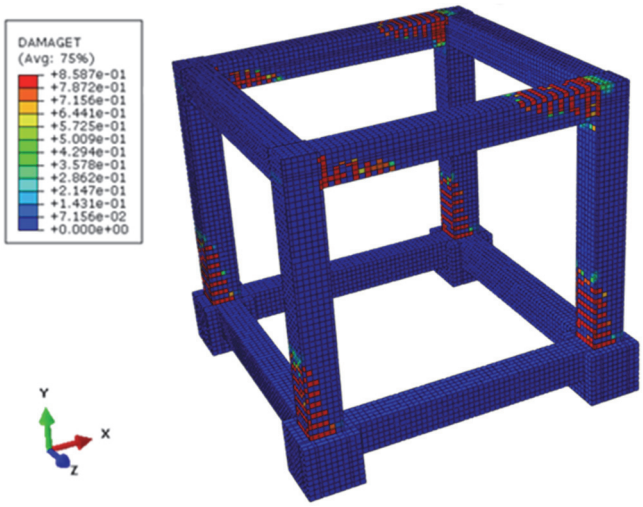

(a)

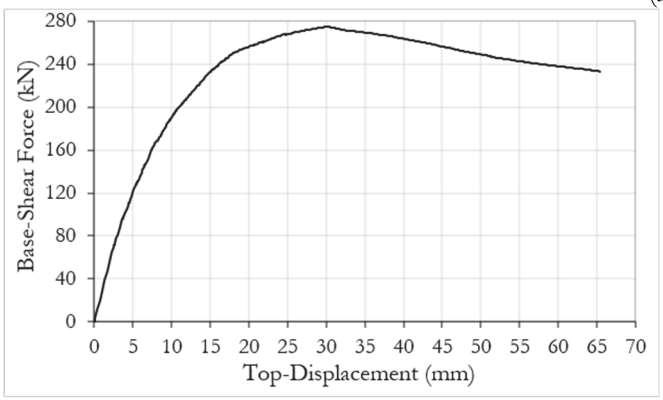

(b)

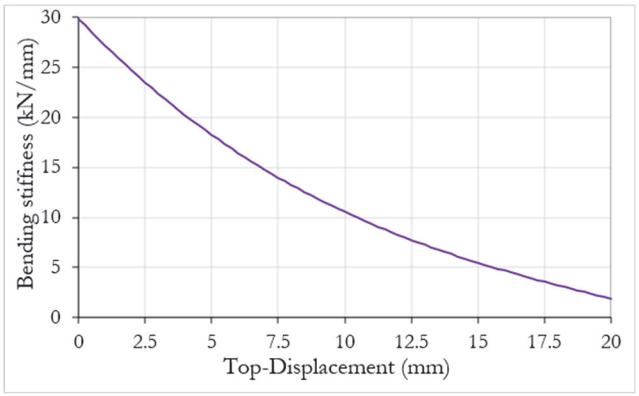

(c)

Figure 6: Product of NSPA (a) Crack propagation (b) Roof-displacement versus Base-shear force and (c) Bending stiffness degradation.

RESULTS

The product of NSPA is illustrated in Fig. 6. The crack propagation as well as the roof displacement versus the base shear force curve, depicted in Fig. 6a, b emphasizes the nonlinear behavior of the RC structure. In general, the numerical test leads to reliable results. In each column, the first and most severe crack transpire at the section just above the base. Afterward, the crack propagates into the section and new cracks appear at higher sections. Meanwhile, in the beams, cracks take place at the sections just beside the connections with columns. The visualization of tensile damage at the final stage demonstrates a spectrum that seems to be realistic. Furthermore, the nonlinear behavior is also observed in Fig. 6b. One of the more prominent takeaways of the line graph is that the nonlinear behavior is appropriate to that of typical RC structures. The product of NSPA initiates with an upward trend in the elastic stage followed by another increasing regime but with a continuous stiffness reduction until hitting peaks starting a declined curve and then ending up at a base shear-force of 85% of the peak. The elastic regime ends up at 11.723 mm and then starts transforming to the nonlinear stage in which the ultimate shear force is determined at 30.218 mm while the fracture occurs at 65.431mm lateral displacement. The displacement ductility factor of the structure is about 4.2 falling into the range of 3 to 6 for typical RC frames according to Park [36]. As a result, it can be concluded that the behavior of the considered RC frame is reliable and can be taken advantage of to evaluate the reducing tendency of its fundamental frequency.

After the determination of the bending capacity based on the base-shear force versus the top lateral displacement graph (Fig. 6b), the stiffness degradation and the reduction of the fundamental frequency of the RC frame can be pointed out rapidly as illustrated in Fig. 6c and Fig. 7, respectively. First of all, the curve that starts from the elastic range to the nonlinear regime until the ultimate point is numerically formulated through an equation. Afterward, the first derivative of this equation at each point stands for the stiffness of the structure at that moment as seen in Fig. 6c. Subsequently, the degraded stiffness corresponding to each level of fault is normalized to the stiffness at the intact state (about 30 kN/mm). Finally, the normalized frequency which is the fraction of the frequency at each loading level to the one determined at the pristine stage is equal to the square root of the normalized stiffness. As a result, the degradation of the first frequency is graphically demonstrated in Fig. 7. It is noted that normalized lateral loading on the horizontal axis is the ratio of the lateral load at each point and the ultimate value.

Compared to the investigation on an RC beam conducted by Hamad et al. [18], the degradation of the fundamental frequency of the considered RC frame is slightly different. For instance, at the moment of 30% of the ultimate load, the declination is 15% for the frame, slightly higher than the 10% value for the beam. When the applied load reaches 70% of the ultimate value, the degradation slightly surpasses 40% for the frame where the amount of reduction of only about 25% is witnessed for the beam. It can be seen that the frequency degradation of the frame seems to be more significant than that of the beam based on the desired moments of loading. In comparison with the approach utilized for the beam, this study gives more sufficient investigation as the fundamental frequency declination can be picturized more thoroughly.

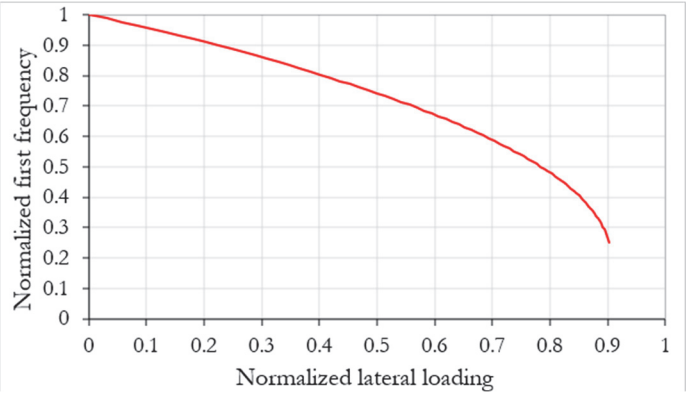

Figure 7: Frequency declination.

The degradation of the first frequency of the RC frame is more extreme as the damage severity increases and can be divided into three main regimes. The modal characteristic decreases about 20% of the counterpart of the pristine frame when the lateral normalized lateral load increase from 0 to 0.4. However, after that, the increase of normalized load from 0.4 to 0.7 causes a degradation of approximately 22%, a more significant reduction compared to the previous state. After this defect

level, extreme degradation of the frequency is witnessed, about 33% when the normalized lateral load is increased by an amount of only 0.2, from 0.7 to 0.9.

Conclusions

The current study numerically evaluates the degradation of the fundamental frequency of an RC frame due to the stiffness declination. In general, the two parameters are proportional to each other but not linearly. The relationship contains some different ranges. It is observed that the first frequency decreases gradually until the lateral load reaches 70% of the ultimate value. At that level of loading, the fundamental frequency lowers to about 60% of the counterpart at the pristine state. From this point, the reduction gets more significant. The coefficient loses an amount of about 30% when increasing the horizontal load from 70% to 90% of the ultimate value. In general, the relationship between the fundamental frequency degradation and fault levels is illustrated effectively and completely using the proposed approach without using data from vibration measurements. The numerical results obtained in this study are useful for further investigation of the effects of damage occurrence on the changes in frequency parameters not only at the fundamental modes but also at higher modes of multiple-storey RC structures. However, the proposed method is only suitable for investigations on each separate mode. The observation in this study is obtained based on the fundamental mode while more slender RC buildings may be damaged at higher modes. Damage may be caused by a single mode or combinations of modes, making the presented method in the current version not adequate.

References

[1] Khatir, A., Capozucca, R., Khatir, S., Magagnini, E. (2022). Vibration-based crack prediction on a beam model using hybrid butterfly optimization algorithm with artificial neural network. Front. Struct. Civ. Eng., 16(8), pp. 976–989. DOI: 10.1007/s11709-022-0840-2.

[2] Ho, L.V., Nguyen, D.H., Mousavi, M., Roeck, G.D., Bui-Tien, T., Gandomi, A.H., Wahab, M.A. (2021). A hybrid computational intelligence approach for structural damage detection using marine predator algorithm and feedforward neural networks, Comput. Struct., 252, 106568. DOI: 10.1016/j.compstruc.2021.106568.

[3] Benaissa, B., Hocine, N.A., Khatir, S., Riahi, M.K., Mirjalili, S. (2021). YUKI Algorithm and POD-RBF for Elastostatic and dynamic crack identification, J. Comput. Sci., 55, 101451. DOI: 10.1016/j.jocs.2021.101451.

[4] Ho, L.V., Trinh, T.T., Roeck, G.D., Bui-Tien, T., Nguyen-Ngoc, L., Wahab, M.A. (2022). An efficient stochastic-based coupled model for damage identification in plate structures, Eng. Fail. Anal., 131, 105866. DOI: 10.1016/j.engfailanal.2021.105866.

[5] Kristiawan, S.A., Hapsari, I.R., Purwanto, E., Marwahyudi, M. (2022). Evaluation of Damage Limit State for RC Frame Based on FE Modeling, Buildings-Basel, 12(1), 21. DOI: 10.3390/buildings12010021.

[6] Khatir, S., Boutchicha, D., Le Thanh, C., Tran-Ngoc, H., Nguyen, T.N., Wahab, M.A. (2020). Improved ANN technique combined with Jaya algorithm for crack identification in plates using XIGA and experimental analysis, Theor. Appl. Fract. Mech., 107, 102554. DOI: 10.1016/j.tafmec.2020.102554.

[7] Khatir, S., Wahab, M.A. (2019). Fast simulations for solving fracture mechanics inverse problems using POD-RBF XIGA and Jaya algorithm, Eng. Fract. Mech., 205, pp. 285–300. DOI: 10.1016/j.engfracmech.2018.09.032.

[8] Thobiani, F.A., Khatir, S., Benaissa, B., Ghandourah, E., Mirjalili, S., Wahab, M.A. (2021). A hybrid PSO and Grey Wolf Optimization algorithm for static and dynamic crack identification. Theor. Appl. Fract. Mech., 118, 103213. DOI: 10.1016/j.tafmec.2021.103213.

[9] Gillich, G.R., Furdui, H., Waha, M.A., Korka, Z.I. (2019). A robust damage detection method based on multi-modalanalysis in variable temperature conditions. Mech. Syst. Signal Proc., 115, pp. 361–379. DOI: 10.1016/j.ymssp.2018.05.037.

[10] Gentile, C., Saisi, A., Cabboi, A. (2015). Structural Identification of a Masonry Tower Based on Operational Modal Analysis, Int. J. Archit. Herit., 9, pp. 98–110. DOI: 10.1080/15583058.2014.951792.

[11] Tiachacht, S., Khatir, S., Le-Thanh, C., Rao, R.V., Mirjalili, S., Wahab, M.A. (2021). Inverse problem for dynamic structural health monitoring based on slime mould algorithm, Eng. Comput., 38, pp. 2205–2228. DOI: 10.1007/s00366-021-01378-8.

[12] Saisi, A., Gentile, C., Guidobaldi, M. (2015). Post-earthquake continuous dynamic monitoring of the Gabbia Tower in Mantua, Italy, Constr. Build. Mater., 81, pp. 101–112. DOI: 10.1016/j.conbuildmat.2015.02.010.

[13] Iacovino, C., Ditommaso, R., Ponzo, F.C., Limongelli, M.P. (2018). The Interpolation Evolution Method for damage localization in structures under seismic excitation, Earthq. Eng. Struct. Dyn., 47(10), pp. 2117-2136. DOI: 10.1002/eqe.3062.
[14] Khatir, S., Tiachacht, S., Thanh, C.L., Ghandourah, E., Mirjalili, S., Wahab, M.A. (2021). An improved Artificial Neural Network using Arithmetic Optimization Algorithm for damage assessment in FGM composite plates, Compos. Struct., 273, 114287. DOI: 10.1016/j.compstruct.2021.114287.
[15] Cerri, M.N., Vestroni, F. (2003). Use of Frequency Change for Damage Identification in Reinforced Concrete Beams, J. Vib. Control, 9(3-4), pp. 475-491. DOI: 10.1177/1077546030307.
[16] Yang, Z., Wang, L. (2010). Structural Damage Detection by Changes in Natural Frequencies, J. Intell. Mater. Syst. Struct., 21(3), pp. 309-319. DOI: 10.1177/1045389X09350332.
[17] Salawu, O.S. (1997). Detection of structural damage through changes in frequency: a review, Eng. Struct., 19(9), pp.718-723. DOI: 10.1016/S0141-0296(96)00149-6.
[18] Hamad, W.I., Owen, J.S., Hussein, M.F.M. (2011). A flexural crack model for damage detection in reinforced concrete structures, J. Phys.: Conf. Ser., 305, 012037. DOI: 10.1088/1742-6596/305/1/012037.
[19] Roumaissa, Z., Khatir, S., Belaidi, I., Le Thanh, C., Wahab, M.A. (2020). A modified transmissibility indicator and Artificial Neural Network for damage identification and quantification in laminated composite structures, Compos. Struct., 248, 112497. DOI: 10.1016/j.compstruct.2020.112497.
[20] Le Thanh, C., Hoang-Le, M., Khatir, S., Wahab, M.A., Tran, M.T., Mirjalili, S. (2021). A novel version of Cuckoo search algorithm for solving optimization problems, Expert Syst. Appl., 186, 115669. DOI: 10.1016/j.eswa.2021.115669.
[21] Saadatmorad, M., Talookolaei, R.-A.J., Pashaei, M.-H., Khatir, S., Wahab, M.A. (2022). Pearson Correlation and Discrete Wavelet Transform for Crack Identification in Steel Beams. Mathematics, 10(15), 2689. DOI: 10.3390/math10152689.
[22] Shirazi, M.I., Khatir, S., Benaissa, B., Mirjalili, S., Wahab, M.A. (2023). Damage assessment in laminated composite plates using modal Strain Energy and YUKI-ANN algorithm, Compos. Struct., 303, 116272. DOI: 10.1016/j.compstruct.2022.116272.
[23] Kupfer, H., Hilsdorf, H.K., Rusch, H. (1969). Behavior of Concrete under Biaxial Stresses, ACI Journal, 66(8): 656-666.
[24] Lubliner, J., Oliver, J., Oller, S., Oñate, E. (1969). A plastic-damage model for concrete. Int. J. Solids Struct., 25(3), pp. 299-326. DOI: 10.1016/0020-7683(89)90050-4.
[25] Batista da Costa, P.O., Bosse, R.M., Gidrão, G.M.S. (2022). Behavior assessment of asymmetrical building with concrete damage plasticity (CDP) under seismic load, Frat. Integrita Strut., 61, pp. 108-118. DOI: 10.3221/IGF-ESIS.61.07.
[26] Nguyen TQ, Livaoğlu R (2020). The effect of the ratio of Λ-shaped shear connectors on the flexural behavior of a reinforced concrete frame, Adv. Struct. Eng., 23(12), pp. 2724-2740. DOI: 10.1177/1369433220920442.
[27] Perera, R., Huerta, C. (2008). Identification of damage in RC beams using indexes based on local modal stiffness, Constr. Build. Mater., 22(8), pp. 1656-1667. DOI: 10.1016/j.conbuildmat.2007.06.012.
[28] Ren, W., Sneed, L.H., Yang, Y., He, R. (2015). Numerical simulation of prestressed precast concrete bridge deck panels using damage plasticity model, Int. J. Concr. Struct. Mater., 9, pp. 45-54. DOI: 10.1007/s40069-014-0091-2.
[29] Najafgholipour, M.A., Dehghan, S.M., Dooshabi, A., Niroomandi, A. (2017). Finite element analysis of RC beam-column connections with governing joint shear failure mode, Lat. Am. J. Solids Struct., 14(7), pp. 1200-1225. DOI: 10.1590/1679-78253682.
[30] Hsu, L.S., Hsu, C.T.T. (1994). Complete stress-strain behavior of high-strength concrete under compression. Mag. Concr. Res., 46(169), pp. 301-312. DOI: 10.1680/macr.1994.46.169.301.
[31] Carreira, D.J., Chu, K.H. (1985). Stress-strain relationship for plain concrete in compression. ACI Journal, 82(6), pp. 797-804.
[32] Aslani, F., Jowkarmeimandi, R. (2012). Stress-strain model for concrete under cyclic loading. Mag. Concr. Res., 64(8), pp. 673-685. DOI: 10.1680/macr.11.00120.
[33] Lee, J., Fenves, G.L. (1998). Plastic-damage model for cyclic loading of concrete structures, J. Eng. Mech., 124(8), pp. 892-900. DOI: 10.1061/(ASCE)0733-9399(1998)124:8(892).
[34] Xiao, Y. (2016). Dynamic behavior of reinforced concrete slabs under rapid loading and low velocity impact. Doctoral thesis, Nanyang Technological University, Singapore.
[35] ACI Committee 374.1, 2005. Acceptance criteria for moment frames based on structural testing and commentary. American Concrete Institute.
[36] Park, R. (1988). State of the art report ductility evaluation from laboratory and analytical testing. Proceeding of Ninth World Conference on Earthquake Engineering, Tokyo-Kyoto, Japan.